A CHARACTERISTICS BASED GENUINELY MULTIDIMENSIONAL DISCRETE KINETIC SCHEME FOR THE EULER EQUATIONS

K. R. ARUN AND M. LUKÁČOVÁ-MEDVIĎOVÁ

Abstract. In this paper we present the results of a kinetic relaxation scheme for an arbitrary hyperbolic system of conservation laws in two space dimensions. We propose a new discrete velocity Boltzmann equation, which is an improvement over the previous models in terms of the isotropic coverage of the multidimensional domain by the foot of the characteristic. The discrete kinetic equation is solved by a splitting method consisting of a convection step and a collision step. The convection step involves only the solution of linear transport equations whereas the collision step instantaneously relaxes the distribution function to a local Maxwellian. An anti-diffusive Chapman-Enskog distribution is used to derive a second order accurate method. Finally some numerical results are presented which confirm the robustness and correct multidimensional behaviour of the proposed scheme.

1. Introduction

The numerical simulation of a hyperbolic system of conservation laws in several space variables is a challenging task. The underlying difficulty is that even for a small initial datum, there is no existence result for a multidimensional Riemann problem needed to construct a numerical approximation. It is well known in the case of a hyperbolic system in general that regardless of the smoothness of the initial datum, the solutions can develop discontinuities in a finite time. The structure of these discontinuities, such as shocks, in multiple dimensions is very complex and resolving them using a numerical scheme is also challenging. Despite all these difficulties, however, the intense research over the past few decades has lead to the development of several numerical methods for solving multidimensional systems of conservation laws. Among the various methods developed so far, the finite volume methods have been the most popular. The main advantages of the finite volume methods are their simplicity and the automatic control of conservation, which is a crucial property. These methods can be broadly classified into two categories: central schemes and upwind schemes.

The central schemes originated as the central finite difference formulation of conservation laws. Some prototypes of these schemes are the Lax-Friedrichs scheme and the Lax-Wendroff scheme. The central schemes are less dependent on the eigenstructure of the conservation laws. However, if no characteristic information is taken into account, the resolution of the numerical scheme may not be satisfactory; particularly when small time steps are enforced by the stability condition. Nonetheless, in recent years, the central schemes have gained a lot of renewed interest due to their new interpretation as Godunov type schemes on both staggered and unstaggered grids. We refer the reader to [29] for a review of central schemes.

The upwind schemes include the Riemann solvers, flux-splitting methods, kinetic theory based methods, recently introduced relaxation schemes [14], etc. Among them, the Riemann solvers and

Date: December 9, 2011.

2010 *Mathematics Subject Classification.* Primary 35L45, 35L60, 35L65, 35L67; Secondary 65M06, 76P05, 82B40.

Key words and phrases. relaxation systems, hyperbolic conservation laws, discrete velocity Boltzmann equation, Maxwellian, Chapman-Enskog distribution.

flux-splitting methods particularly make use of quasi-dimensional splitting and the solution of one-dimensional (1-D) Riemann problems. If one is interested to approximate only some features that are just 1-D, these schemes can produce good qualitative results. However, for complex genuinely multidimensional structures, such as oblique shocks or circular expansions, the dimensional splitting approach can yield spurious local wave structure resolutions, e.g. see [18, 23, 27, 28]. This led to the development of the so-called genuinely multidimensional numerical methods for solving systems of conservation laws in several space variables. Looking back to the literature, we can find several genuinely multidimensional methods: the wave residual method due to Roe [27], the method of transport due to Fey [10] and its improved version due to Noelle [22], the wave propagation algorithm of LeVeque [17], the finite volume evolution Galerkin scheme due to Lukáčová and collaborators [2, 20], to name but a few.

An important category of upwind methods is the kinetic schemes, which are based on the Boltzmann equation of kinetic theory. The kinetic schemes exploit the fact that the physical systems of conservation laws arising in continuum mechanics can be obtained as an appropriate limit of the various moments of the Boltzmann equation [6]. One of the most fascinating features of the kinetic schemes is that when applied to the Euler equations of gas dynamics, they preserve the positivity of mass density and pressure. As a result, the kinetic schemes are unconditionally stable in the L^1-norm. Moreover, the kinetic schemes are entropy stable as a consequence of the celebrated Boltzmann H-theorem and they also enjoy the property of being genuinely multidimensional. For a review of kinetic schemes we refer the reader to [9, 11, 25, 26, 31] and the references cited therein.

Recently, Jin and Xin [14] introduced a new category of upwind methods called relaxation schemes, based on the relaxation approximation of conservation laws. In this method, the given nonlinear system of conservation laws is replaced by a larger semi-linear system known as the relaxation system. The relaxation system has a stiff source term containing a small relaxation parameter ϵ. The original system of conservation laws can be recovered from the relaxation system in the limit as $\epsilon \to 0$. In [14] Jin and Xin have developed a variety of numerical schemes which are classified into two categories: relaxing schemes and relaxed schemes. The relaxing schemes are obtained by directly discretising the relaxation system and hence they contain the stiff parameter ϵ explicitly. A relaxed scheme is the limit of a relaxing scheme when $\epsilon = 0$. Due to the presence of ϵ, it is in general difficult to attain high order time accuracy in relaxing schemes. Nevertheless, special Runge-Kutta time stepping schemes with appropriate MUSCL or WENO type space discretisations have been proposed in [13, 14, 24], to develop high order relaxing schemes.

A new interpretation of a relaxation system in the form of a discrete velocity model of the Boltzmann equation has been proposed in [1, 5]. One of the important aspects of this correspondence is that we can exploit the vast literature of kinetic theory and develop relaxation schemes which possess all the desired properties of kinetic schemes, such as the positivity preservation, entropy stability, genuine multidimensional nature, etc. The goal of the present work is to make use of this analogy and to develop a genuinely multidimensional relaxation scheme for the compressible Euler equations in two space dimensions. The main advantages of the discrete Boltzmann model are the linearity of the convective part, simplicity compared to classical Boltzmann equation, diagonal form of the flux Jacobian matrices and the ease for upwinding. We solve the discrete Boltzmann equation by a splitting method consisting of a convection phase and a collision phase. The convection phase involves only the solution of linear transport equations and the collision phase instantaneously relaxes the distribution function to an equilibrium distribution. However, as pointed out in [13], such a simple splitting strategy reduces the resulting numerical scheme to formally first order accurate in time. Moreover, the first order scheme suffers from a large amount of numerical dissipation. Nonetheless, in the context of classical kinetic schemes, Deshpande [8] had already circumvented these difficulties by the use of an anti-diffusive Chapman-Enskog distribution instead of

the Maxwellian. Recently, Kunik et al. [15] also employed same mechanism to design a second order kinetic scheme for the relativistic hydrodynamics equations. Along similar lines of [8, 15], we derive an anti-diffusive Chapman-Enskog distribution for the discrete Boltzmann equation to develop a second order upwind relaxation scheme. It is to be remarked that the Chapman-Enskog method is always associated with nonlinear convection-diffusion equations [6] and the use of Chapman-Enskog distribution function to reduce the excess numerical diffusion in the first order relaxation scheme is novel. Moreover, our scheme avoids intricate and time consuming solving of Riemann problems and complicated flux-splittings. In [3] we have already introduced a second order accurate 1-D relaxation scheme with the use of Chapman-Enskog distribution and the present work is its genuine multidimensional extension to the two-dimensional (2-D) case. Our scheme uses the discrete velocity Boltzmann equation, appropriate equilibrium distributions, characteristics and interpolation. This makes our approach different from the conventional relaxation schemes.

The paper is organised as follows. In section 2 we introduce a relaxation system for the Euler equations of gas dynamics in the form of a discrete velocity Boltzmann equation. The first order accurate numerical scheme and its properties are presented in section 3. In section 4 we extend the first order scheme to second order with aid of an anti-diffusive Chapman-Enskog distribution. The section 5 is devoted to the results of numerical experiments. Finally, we conclude the paper with some remarks in section 6.

2. Relaxation Systems for Conservation Laws

In this section we introduce a relaxation system for the 2-D compressible Euler equations of an ideal gas in the form of a discrete velocity Boltzmann equation. However, we follow a general approach and therefore, the present ideas can be easily extended to any complex system of conservation laws. The Euler equations forms a nonlinear hyperbolic system of conservation laws which represents the fundamental conservation principles of mass, momentum and energy, given by

$$\frac{\partial w}{\partial t} + \frac{\partial g_1(w)}{\partial x} + \frac{\partial g_2(w)}{\partial y} = 0, \tag{2.1}$$

where the vector of conserved variables w, the flux-vectors $g_1(w)$ and $g_2(w)$ are given as

$$w = \begin{pmatrix} \rho \\ \rho u \\ \rho v \\ E \end{pmatrix}, \; g_1(w) = \begin{pmatrix} \rho u \\ \rho u^2 + p \\ \rho uv \\ (E+p)u \end{pmatrix}, \; g_2(w) = \begin{pmatrix} \rho v \\ \rho uv \\ \rho v^2 + p \\ (E+p)v \end{pmatrix}. \tag{2.2}$$

Here, ρ is the density, ρu and ρv are respectively the momentum components in x- and y-directions and E is the total energy given by

$$E = \rho e + \frac{1}{2}\rho\left(u^2 + v^2\right), \tag{2.3}$$

where e is the internal energy density, which is related to the pressure p via the relation

$$p = (\gamma - 1)\rho e. \tag{2.4}$$

In the sequel, we shall frequently denote the momentum components by m and n, i.e. $(m, n) = (\rho u, \rho v)$. Since ρ and p represents the mass density and pressure, they remain positive always. Thus, the state space for the system (2.1), the so-called admissible space, is the set

$$\mathcal{W} := \left\{ (\rho, m, n, E) \in \mathbb{R}^4 \colon \rho > 0, E - \frac{1}{2\rho}\left(m^2 + n^2\right) > 0 \right\}. \tag{2.5}$$

The following proposition follows immediately.

Proposition 2.1. *The set $\mathcal{W}$ has the property: if $w_1, w_2 \in \mathcal{W}$ and $\alpha_1, \alpha_2 > 0$, then $\alpha_1 w_1 + \alpha_2 w_2 \in \mathcal{W}$. In particular, $\mathcal{W}$ is a convex set.*

A relaxation phenomenon arises when the equilibrium state of a physical system is perturbed. One of the most common occurrences of relaxation processes is in rarefied gas dynamics which is represented by the well known Boltzmann equation, see [6]. The Boltzmann equation for a monatomic perfect gas in two space dimensions is given by

$$\frac{\partial f}{\partial t} + \mathbf{k} \cdot \nabla_{\mathbf{x}} f = \frac{1}{\epsilon} Q(f), \tag{2.6}$$

where $f(\mathbf{x}, t, \mathbf{k})$ is the particle density function, which depends on the phase-space coordinates $\mathbf{x} = (x, y), \mathbf{k} = (k_1, k_2)$ and the time t. The macroscopic conserved variables, the mass, momenta and energy are defined as the moments of f, i.e.

$$w(\mathbf{x}, t) := \int_{\mathbb{R}^2} \psi(\mathbf{k}) f(\mathbf{x}, t, \mathbf{k}) d\mathbf{k}, \tag{2.7}$$

where

$$\psi(\mathbf{k}) = \begin{pmatrix} 1 \\ \mathbf{k} \\ \frac{1}{2}\mathbf{k}^2 \end{pmatrix}. \tag{2.8}$$

The Boltzmann collision operator Q consists of a very complex integral term. An interesting property of the collision operator is that $Q(f) = 0$ if and only if f is the Maxwellian, i.e.

$$f(\mathbf{x}, t, \mathbf{k}) = M(w, \mathbf{k}) := \frac{\rho}{2\pi\vartheta} e^{-\frac{\left(|k_1 - u|^2 + |k_2 - v|^2\right)}{2\vartheta}}, \tag{2.9}$$

where ϑ denotes the temperature. In their work [4], Bhatnagar et al. introduced a simple model for Q based on the relaxation process of a swarm of molecules towards an equilibrium state. This led to the so-called BGK model of the Boltzmann equation (2.6), which reads

$$\frac{\partial f}{\partial t} + \mathbf{k} \cdot \nabla_{\mathbf{x}} f = \frac{1}{\epsilon} \left(M(w_f, \mathbf{k}) - f \right). \tag{2.10}$$

Here, $\epsilon > 0$ is a small parameter known as the relaxation time and w_f is defined by (2.7) as a moment of f.

The BGK Boltzmann equation (2.10) facilitated the development of kinetic schemes, which have been very successful in the numerical modelling of many initial and boundary value problems in fluid dynamics. These kinetic schemes are based on the fact that the Euler equations (2.1) are the first moments of the Boltzmann equation (2.6) when the distribution function is the Maxwellian (2.9), see [9, 11, 25, 26, 31] for more details. The kinetic schemes possess many fascinating features: robustness, upwind bias, preservation of the positivity of mass density and pressure, entropy stability, etc.

As a generalisation of kinetic BGK models, in [5] Bouchut has introduced a general framework for constructing a BGK model for any system of conservation laws endowed with a convex entropy. An important feature of this formulation is that the constructed BGK model possesses a large family of kinetic entropies. There exists an analogue of the classical Boltzmann H-theorem [6], the exploitation of which yields the entropy inequality in the hydrodynamic limit, see [5] for more details. In this work we use the discrete velocity relaxation model introduced in [1, 5]. The BGK equation then reads

$$\frac{\partial f_k}{\partial t} + a_1(k) \frac{\partial f_k}{\partial x} + a_2(k) \frac{\partial f_k}{\partial y} = \frac{1}{\epsilon} \left(M_k(w_f) - f_k \right) \tag{2.11}$$

for $k \in \{1, 2, \ldots, N\}$. Here $f_k = f_k(x, y, t) \in \mathbb{R}^4$ is unknown, $(a_1(k), a_2(k)) \in \mathbb{R}^2$ is a constant, $w_f = \sum_{k=1}^N f_k$ and the so-called Maxwellian $M_k \colon \mathcal{W} \to \mathbb{R}^4$ satisfy the consistency conditions

$$\sum_{k=1}^N M_k(w) = w, \ \sum_{k=1}^N a_1(k) M_k(w) = g_1(w), \ \sum_{k=1}^N a_2(k) M_k(w) = g_2(w). \tag{2.12}$$

The conditions (2.12) are the necessary conditions for the BGK model (2.11) to converge to the Euler equations (2.1) in the limit $\epsilon \to 0$, see also [1, 21] for more details. We note that the BGK model (2.11) is completely determined once the discrete velocities $(a_1(k), a_2(k))$ and the Maxwellian M_k are obtained. The choices of $(a_1(k), a_2(k))$ and M_k are to be done according to some suitable stability conditions. It is well known that even for general relaxation models [7, 19, 21] an approximation of the type (2.11) has to obey some stability criterion so as to possess the correct hydrodynamic limit, e.g. in the case of 2×2 relaxation systems the well known sub-characteristic condition [7, 19] has to be satisfied. We use the entropy extension condition of Bouchut [5] so that the BGK model (2.11) is compatible with the entropies of (2.1). The main result of [5] for the discrete velocity BGK models of the type (2.11) states: under the necessary and sufficient condition

$$\sigma(M_k'(w)) \subset [0, \infty) \ \forall k, \tag{2.13}$$

corresponding to any entropy $h(w)$ of (2.1), there exist a kinetic entropy $H_k(f_k)$ of (2.11) such that

(i) H_k is a convex function,

(ii) $\sum_{k=1}^N H_k(M_k(w)) = h(w)$,

(iii) $\sum_{k=1}^N H_k(M_k(w_f)) \leq \sum_{k=1}^N H_k(f_k)$.

We now proceed to give the explicit expressions for the discrete velocities $a(k)$ and the Maxwellian M_k in accordance with the stability requirement (2.13). Henceforth, we take $N = 4$ and make a symmetric choice

$$\begin{aligned} &(a_1(1), a_2(1)) = (-\lambda, -\lambda), \quad &&(a_1(2), a_2(2)) = (\lambda, -\lambda), \\ &(a_1(3), a_2(3)) = (\lambda, \lambda), &&(a_1(4), a_2(4)) = (-\lambda, \lambda), \end{aligned} \tag{2.14}$$

where λ is a parameter to be determined. In order to satisfy (2.13), we choose M_k to be a linear combination of $w, g_1(w)$ and $g_2(w)$, i.e.

$$M_k(w) = \alpha_0(k) w + \alpha_1(k) g_1(w) + \alpha_2(k) g_2(w). \tag{2.15}$$

With the aid of (2.14), the relations (2.12) immediately give the expressions

$$\begin{aligned} M_1(w) &= \frac{w}{4} - \frac{g_1(w)}{4\lambda} - \frac{g_2(w)}{4\lambda}, \quad &M_2(w) &= \frac{w}{4} + \frac{g_1(w)}{4\lambda} - \frac{g_2(w)}{4\lambda}, \\ M_3(w) &= \frac{w}{4} + \frac{g_1(w)}{4\lambda} + \frac{g_2(w)}{4\lambda}, \quad &M_4(w) &= \frac{w}{4} - \frac{g_1(w)}{4\lambda} + \frac{g_2(w)}{4\lambda}. \end{aligned} \tag{2.16}$$

The expression for the parameter λ can now be easily obtained. Since the eigenvalues of the Jacobian of $g_1(w)$ and $g_2(w)$ are known, the condition (2.13) can be exactly evaluated to yield

$$\lambda = \| |u| + |v| + \sqrt{2} a \|_\infty, \tag{2.17}$$

where a denotes the sound speed.

Remark 2.2. If we assume that the functions $M_k(w)$ are continuously differentiable, then $\{M_k(w)\}$ gives a wavemodel [22] for the system (2.1) with $(a_1(k), a_2(k))$ as the corresponding advection velocities. The relation (2.12) precisely shows that this wavemodel is consistent with both the

statevector w and the fluxvectors $g_1(w)$ and $g_2(w)$. In other words, we can decompose the statevector w into N (in our case $N=4$) waves $M_k(w)$ which advect with velocities $(a_1(k), a_2(k))$.

In the following lemma we prove that the Maxwellian $M_k \colon \mathcal{W} \to \mathbb{R}^4$ maps $\mathcal{W}$ to itself. This lemma is very useful in the numerical approximation stage.

Lemma 2.3. *The Maxwellian M_k leaves the domain $\mathcal{W}$ to be invariant, i.e. $M_k(w) \in \mathcal{W}$, whenever $w \in \mathcal{W}$.*

Proof. For $w = (\rho, m, n, E) \in \mathbb{R}^4$ we define

$$\hat{\rho}(w) := \rho, \ \hat{p}(w) := E - \frac{m^2+n^2}{2\rho}. \tag{2.18}$$

Therefore, $w \in \mathcal{W}$ is equivalent to $\hat{\rho}(w) > 0$ and $\hat{p}(w) > 0$. Now,

$$\begin{aligned} \hat{\rho}\left(\frac{w}{4} \pm \frac{g_1(w)}{4\lambda} \pm \frac{g_2(w)}{4\lambda}\right) &= \frac{\rho}{4} \pm \frac{\rho u}{4\lambda} \pm \frac{\rho v}{4\lambda} \\ &= \frac{\rho}{4}\left(1 \pm \frac{u}{\lambda} \pm \frac{v}{\lambda}\right) \end{aligned} \tag{2.19}$$

and the right hand side of (2.19) is clearly positive under the stability condition (2.17). Thus, the density part of M_k is positive. We can now show that the pressure part is positive.

$$\begin{aligned} \hat{p}\left(\frac{w}{4} \pm \frac{g_1(w)}{4\lambda} \pm \frac{g_2(w)}{4\lambda}\right) &= \frac{E}{4} \pm \frac{(E+p)u}{4\lambda} \pm \frac{(E+p)v}{4\lambda} \\ &\quad - \frac{\left\{\frac{m}{4} \pm \frac{\left(\frac{m^2}{\rho}+p\right)}{4\lambda} \pm \frac{\left(\frac{mn}{\rho}\right)}{4\lambda}\right\}^2 + \left\{\frac{n}{4} \pm \frac{\left(\frac{mn}{\rho}\right)}{4\lambda} \pm \frac{\left(\frac{n^2}{\rho}+p\right)}{4\lambda}\right\}^2}{2\left(\frac{\rho}{4} \pm \frac{\rho u}{4\lambda} \pm \frac{\rho v}{4\lambda}\right)} \\ &= \frac{E}{4}\left(1 \pm \frac{u}{\lambda} \pm \frac{v}{\lambda}\right) \pm \left(\frac{pu}{4\lambda} + \frac{pv}{4\lambda}\right) \\ &\quad - \frac{\left\{\frac{m}{4}\left(1 \pm \frac{u}{\lambda} \pm \frac{v}{\lambda}\right) \pm \frac{p}{4\lambda}\right\}^2 + \left\{\frac{n}{4}\left(1 \pm \frac{u}{\lambda} \pm \frac{v}{\lambda}\right) \pm \frac{p}{4\lambda}\right\}^2}{\frac{\rho}{2}\left(1 \pm \frac{u}{\lambda} \pm \frac{v}{\lambda}\right)} \\ &= \frac{1}{4}\left(1 \pm \frac{u}{\lambda} \pm \frac{v}{\lambda}\right)\left\{E - \frac{m^2+n^2}{2\rho}\right\} - \frac{p^2}{4\lambda^2\rho\left(1 \pm \frac{u}{\lambda} \pm \frac{v}{\lambda}\right)} \\ &= \frac{1}{4}\left(1 \pm \frac{u}{\lambda} \pm \frac{v}{\lambda}\right)\left\{1 - \frac{p^2}{\rho^2 e(\lambda \pm u \pm v)^2}\right\}\rho e. \end{aligned} \tag{2.20}$$

It can easily be seen that the quantity in the curly brackets remains positive under the stability criterion (2.17). Hence, the pressure part of M_k is also positive and this completes the proof. □

3. Kinetic Relaxation Scheme

In this section we derive a discrete kinetic scheme for the Euler equations (2.1) using the discrete velocity Boltzmann equation (2.11). In the first step, we start with a bounded, integrable initial data for the macroscopic variables, i.e.

$$\rho(x,y,0) > 0, \ u(x,y,0), \ v(x,y,0), \ p(x,y,0) > 0. \tag{3.1}$$

Let $0 = t^0 < t^1 < \cdots < t^n < \cdots$ be an increasing sequence of times. We denote the solution at time $t = t^n$ by $w^n(x,y)$, i.e. $w^n(x,y) \sim w(x,y,t^n)$. Given the values of $w^n(x,y)$, we compute λ from (2.17) and form the Maxwellian densities $M_k(w^n(x,y))$. We assume that the distribution function relaxes instantaneously to the Maxwellian at time $t = t^n$, i.e. $f_k(x,y,t^n) = M_k(w^n(x,y))$. This

process has been referred to as collision phase in the literature of classical kinetic schemes [8]. In the next stage we solve an initial value problem for the collision-free Boltzmann equation

$$\frac{\partial f_k}{\partial t} + a_1(k)\frac{\partial f_k}{\partial x} + a_2(k)\frac{\partial f_k}{\partial y} = 0, \tag{3.2}$$

$$f_k(x, y, t^n) = M_k(w^n(x, y)). \tag{3.3}$$

Let $t^{n+1} = t^n + \Delta t^n$. The initial value problem (3.2)-(3.3) can be solved exactly to get the solution

$$\begin{aligned} f_k(x, y, t^{n+1}) &= f_k(x - a_1(k)\Delta t^n, y - a_2(k)\Delta t^n, t^n) \\ &= M_k\left(w^n(x - a_1(k)\Delta t^n, y - a_2(k)\Delta t^n)\right). \end{aligned} \tag{3.4}$$

This leads to an iterative scheme for the macroscopic conserved variable w, defined via

$$w^{n+1}(x, y) = \sum_{k=1}^{4} M_k\left(w^n(x - a_1(k)\Delta t^n, y - a_2(k)\Delta t^n)\right). \tag{3.5}$$

Thus, our numerical scheme consists of two steps: a collision phase and a convection phase. In the collision phase the distribution function f_k relaxes instantaneously to the equilibrium distribution $M_k(w)$. It tantamount to performing particle collisions instantaneously to make the transition from a non-equilibrium state to an equilibrium state. On the other hand, the convection phase drives the system away from the equilibrium state, i.e. f_k becomes different from the equilibrium M_k. Therefore, our numerical scheme (3.5), derived in the spirit of kinetic schemes, is termed as kinetic relaxation scheme.

Remark 3.1. It has to be noted that the scheme (3.5) is discrete in time, but continuous in space. Further, it is unconditionally stable, i.e. it does not require any restriction on the timestep Δt^n. However, as mentioned in [5], the simple splitting strategy we have employed here reduces the time accuracy of the scheme to just first order. This follows easily from the calculation of truncation error for (3.5).

We now proceed to discretise (3.5) in an upwind fashion to derive a fully discrete scheme. As a first step, we introduce a mesh, which for simplicity is assumed to be uniform with mesh sizes Δx and Δy respectively in x- and y-directions. In the following, we shall always abbreviate by $\phi^n_{i,j}$, the approximation to the value of a grid function ϕ at a point (x_i, y_j) at time t^n, i.e. $\phi^n_{i,j} \sim \phi(x_i, y_j, t^n)$.

Using $a_1(1) = -\lambda, a_2(1) = -\lambda, \lambda > 0$ we get from (3.4)

$$f_1(x, y, t^{n+1}) = M_1(w^n(x_i + \lambda\Delta t^n, y_j + \lambda\Delta t^n)). \tag{3.6}$$

Since the values of M_1 are available only at the mesh points, we need to use some interpolation to compute the right hand side expression in (3.6), see Figure 1.

The upwind schemes are based on the inherent signal or wave propagation property of the hyperbolic equations. In multidimensional cases, the signals come from infinitely many directions and hence a numerical scheme should also take the information from all directions into account. However, the traditional upwind schemes consider the only the waves propagating in the coordinate directions and therefore they are typically grid dependent. This means that in the interpolation needed in (3.6), a grid-aligned upwind scheme would suggest to use the values of M_1 at the three points A, B and D and ignore the contribution from the cross wind direction C to get

$${f_1}^{n+1}_{i,j} = {M_1}^n_{i,j} + \eta_1\delta_x^+ M_{1i,j} + \eta_2\delta_y^+ M_{1i,j}, \tag{3.7}$$

where $\eta_1 := \lambda\Delta t^n/\Delta x$ and $\eta_2 := \lambda\Delta t^n/\Delta y$ are the mesh ratios and δ_x^+ is the forward difference operator defined by

$$\delta_x^+\phi(x, y) := \phi(x + \Delta x, y) - \phi(x, y) \tag{3.8}$$

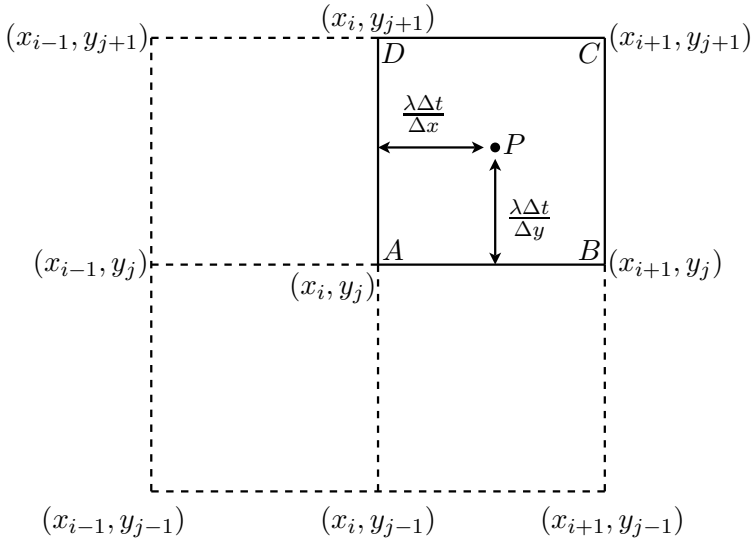

FIGURE 1. Nine-point stencil used for interpolation

with an analogous definition for δ_y^+. However, as already mentioned in the introduction, this approach will typically result in a bad smearing of the flow features which are oblique to the grid.

The success of a well conceived genuinely multidimensional scheme depends on how accurately the information from all the directions is taken into account. In our scheme, instead of accessing the points via grid-aligned upwinding, we interpolate using the point values from all the four points A, B, C and D in the stencil. In this way, our algorithm naturally leads to a genuinely multi-dimensional approach and avoids the dimension-by-dimension treatment. Thus, using a bilinear interpolation instead of (3.7), we get

$$f_{1_{i,j}}^{n+1} = M_{1_{i,j}}^n + \eta_1 \delta_x^+ M_{1_{i,j}}^n + \eta_2 \delta_y^+ M_{1_{i,j}}^n + \eta_1 \eta_2 \delta_x^+ \delta_y^+ M_{1_{i,j}}^n. \tag{3.9}$$

Employing analogous interpolations for other distribution functions we can obtain

$$f_{2_{i,j}}^{n+1} = M_{2_{i,j}}^n - \eta_1 \delta_x^- M_{2_{i,j}}^n + \eta_2 \delta_y^+ M_{2_{i,j}}^n - \eta_1 \eta_2 \delta_x^- \delta_y^+ M_{2_{i,j}}^n, \tag{3.10}$$

$$f_{3_{i,j}}^{n+1} = M_{3_{i,j}}^n - \eta_1 \delta_x^- M_{3_{i,j}}^n - \eta_2 \delta_y^- M_{3_{i,j}}^n + \eta_1 \eta_2 \delta_x^- \delta_y^- M_{3_{i,j}}^n, \tag{3.11}$$

$$f_{4_{i,j}}^{n+1} = M_{4_{i,j}}^n + \eta_1 \delta_x^+ M_{4_{i,j}}^n - \eta_2 \delta_y^- M_{4_{i,j}}^n - \eta_1 \eta_2 \delta_x^+ \delta_y^- M_{4_{i,j}}^n. \tag{3.12}$$

Finally, the fully discrete iterative scheme reads

$$w_{i,j}^{n+1} = \sum_{k=1}^{4} f_{k_{i,j}}^{n+1}. \tag{3.13}$$

The rest of this section is devoted to the analysis of the scheme (3.13). The main results are summarised in the following theorem.

Theorem 3.2. *Under the CFL condition*

$$\frac{\lambda\Delta t^n}{\Delta x} < 1, \frac{\lambda\Delta t^n}{\Delta y} < 1, \tag{3.14}$$

the iterative scheme (3.13) *possesses the following features:*

(1) *the discrete conservation property, i.e.*

$$\sum_{i,j\in\mathbb{Z}} w_{i,j}^{n+1} = \sum_{i,j\in\mathbb{Z}} w_{i,j}^{n}, \tag{3.15}$$

(2) *preserves the positivity of density and pressure, i.e.*

$$\rho_{i,j}^{n} > 0,\ p_{i,j}^{n} > 0\ \forall i,j\in\mathbb{Z} \implies \rho_{i,j}^{n+1} > 0,\ p_{i,j}^{n+1} > 0,\ \forall i,j\in\mathbb{Z}. \tag{3.16}$$

(3) *entropy property, i.e. for any convex entropy h of the Euler equations* (2.1) *we have the inequality*

$$\sum_{i,j\in\mathbb{Z}} h\left(w_{i,j}^{n+1}\right) \leq \sum_{i,j\in\mathbb{Z}} h\left(w_{i,j}^{n}\right). \tag{3.17}$$

Proof. (1) We make use of the interpolation formulae (3.9)-(3.12) on the right hand side of (3.13) and recast the resulting expression as a nine-point difference scheme

$$w_{i,j}^{n+1} = \sum_{k=1}^{4} \sum_{i',j'=-1}^{1} \alpha_{i',j'}^{(k)} M_k{}_{i+i',j+j'}^{n}, \tag{3.18}$$

where the coefficients $\alpha_{i',j'}^{(k)}$ satisfy

$$\sum_{i',j'=-1}^{1} \alpha_{i',j'}^{(k)} = 1,\ k = 1,2,3,4. \tag{3.19}$$

Since $\sum_{k=1}^{4} M_k(w) = w$, the discrete conservation property (3.15) follows very easily by summing (3.18) over $i,j\in\mathbb{Z}$ and using (3.19).

(2) In the light of (3.19) we observe that for each $k = 1,2,3,4$, the right side expression in (3.18) is a convex linear combination of the $M_k{}_{i,j}^{n}$. In lemma 2.3 we have already proved that $M_k(w)\in\mathcal{W}$ whenever $w\in\mathcal{W}$. Hence, each of four summands with respect to k is in $\mathcal{W}$. This in turn shows that their sum also belongs to $\mathcal{W}$, in view of the proposition 2.1.

(3) As mentioned in section 2, corresponding to any convex entropy h of (2.1), there exists a kinetic entropy H_k so that

$$\begin{aligned} h\left(w_{i,j}^{n+1}\right) &= \sum_{k=1}^{4} H_k\left(w_{i,j}^{n}\right) \\ &\leq \sum_{k=1}^{4} H_k\left(f_k{}_{i,j}^{n+1}\right) \\ &= \sum_{k=1}^{4} H_k\left(\sum_{i',j'=-1}^{1} \alpha_{i',j'}^{(k)} M_k{}_{i+i',j+j'}^{n}\right) \\ &\leq \sum_{k=1}^{4} \sum_{i',j'=-1}^{1} \alpha_{i',j'}^{(k)} H_k\left(M_k{}_{i+i',j+j'}^{n}\right), \end{aligned} \tag{3.20}$$

where the last inequality follows by using Jensen's inequality for convex functions. The entropy inequality now easily follows from (3.20) by summation and using (3.19).

□

Remark 3.3. The positivity of the mass density and pressure is intimately related to the L^1 stability of the scheme. Since the quantities ρ and E remain positive and the scheme is conservative, we have

$$\begin{aligned}\|\rho^{n+1}\|_{L^1} &= \sum_{i,j\in\mathbb{Z}} \rho_{i,j}^{n+1} \\ &= \sum_{i,j\in\mathbb{Z}} \rho_{i,j}^{n} \\ &= \|\rho^n\|_{L^1}.\end{aligned}$$

In an analogous manner we can show

$$\|E^{n+1}\|_{L^1} = \|E^n\|_{L^1}.$$

For the momentum we obtain

$$\begin{aligned}\|\rho^{n+1}u^{n+1}\|_{L^1} &= \sum_{i,j\in\mathbb{Z}} \rho_{i,j}^{n+1}|u|_{i,j}^{n+1} \\ &= \sum_{i,j\in\mathbb{Z}} \left(\rho_{i,j}^{n+1}\right)^{1/2} \left(\rho_{i,j}^{n+1}\left(u_{i,j}^{n+1}\right)^2\right)^{1/2} \\ &\le \left(\sum_{i,j\in\mathbb{Z}} \rho_{i,j}^{n+1}\right)^{1/2} \left(\sum_{i,j\in\mathbb{Z}} \rho_{i,j}^{n+1}\left(u_{i,j}^{n+1}\right)^2\right)^{1/2} \\ &\le 2\|\rho^{n+1}\|_{L^1}^{1/2} \left(\sum_{i,j\in\mathbb{Z}} E_{i,j}^{n+1}\right)^{1/2} \\ &= 2\|\rho^{n+1}\|_{L^1}^{1/2}\|E^{n+1}\|_{L^1}^{1/2} \\ &= 2\|\rho^{n}\|_{L^1}^{1/2}\|E^{n}\|_{L^1}^{1/2} \\ &\le \|\rho^n\|_{L^1} + \|E^n\|_{L^1}.\end{aligned}$$

Analogous inequalities can be derived also for the y-momentum ρv. Hence, we have established the L^1 stability of the difference scheme (3.13).

4. Second Order Accurate Kinetic Relaxation Scheme

In this section we present an extension of the first order scheme (3.5) to second order. As already mentioned in the introduction, our approach is along the lines of that advocated by Deshpande [8]. Even though the first order fully discrete scheme (3.13) has many desirable properties, such as conservativity, positivity preservation and entropy stability, however, it suffers from a large amount of numerical dissipation. We shall see later in this section that the numerical dissipation of the first order discrete kinetic scheme (3.13) is proportional to the timestep Δt^n. Following Deshpande [8], we employ a Chapman-Enskog type expansion to derive a higher order numerical dissipation. With the aid of this mechanism the resulting numerical scheme not only achieves overall second order time accuracy, but also reduces the excess numerical dissipation.

There are two steps in deriving a second order scheme. In the first step, we proceed to achieve second order accuracy in time. For this we employ the Chapman-Enskog type procedure, which leads to an anti-diffusive flux correction strategy. The second step is to achieve second order accuracy in space, which consists of using a second order interpolation method.

4.1. **Second Order Accuracy in Time.** Expanding the exact solution $w(x,y,t)$ in the Taylor series to second order accuracy yields

$$w(x,y,t^n+\Delta t^n) = w(x,y,t^n) + \Delta t^n \frac{\partial w}{\partial t}(x,y,t^n) + \frac{(\Delta t^n)^2}{2}\frac{\partial^2 w}{\partial t^2}(x,y,t^n) + \mathcal{O}\left((\Delta t^n)^3\right). \tag{4.1}$$

We make use of the conservation law (2.1) to replace the time derivatives of w by space derivatives to obtain

$$\begin{aligned} w(x,y,t^n+\Delta t^n) = w(x,y,t^n) - \Delta t^n \left(\frac{\partial g_1}{\partial x} + \frac{\partial g_2}{\partial y}\right)(x,y,t^n) + \frac{(\Delta t^n)^2}{2}\left\{\frac{\partial}{\partial x}\left(A_1^2\frac{\partial w}{\partial x} + A_1A_2\frac{\partial w}{\partial y}\right)\right. \\ \left. + \frac{\partial}{\partial y}\left(A_2A_1\frac{\partial w}{\partial x} + A_2^2\frac{\partial w}{\partial y}\right)\right\}(x,y,t^n) + \mathcal{O}\left((\Delta t^n)^3\right), \end{aligned} \tag{4.2}$$

where we have denoted $A_1(w) = \partial g_1/\partial w$ and $A_2(w) = \partial g_2/\partial w$, the flux Jacobian matrices. Our aim is to compare (4.2) with a corresponding second order Taylor expansion of the right hand side of (3.5). This comparison will give us the missing terms in the first order kinetic relaxation scheme, the so-called anti-diffusive terms. In order to proceed, we first expand the summands on the right hand side of (3.5) to second order accuracy, resulting in

$$\begin{aligned} M_k((w^n(x-a_1(k)\Delta t^n, y-a_2(k)\Delta t^n)) = M_k\left(w^n(x,y)\right) - \Delta t^n\left(a_1(k)\frac{\partial}{\partial x} + a_2(k)\frac{\partial}{\partial y}\right)M_k\left(w^n(x,y)\right) \\ + \frac{(\Delta t^n)^2}{2}\left(a_1(k)\frac{\partial}{\partial x} + a_2(k)\frac{\partial}{\partial y}\right)^2 M_k\left(w^n(x,y)\right) \\ + \mathcal{O}((\Delta t^n)^3). \end{aligned} \tag{4.3}$$

Taking the moments, i.e. summing over k and using the relations (2.12) yields

$$\begin{aligned} w(x,y,t^n+\Delta t^n) = w(x,y,t^n) - \Delta t^n\left(\frac{\partial g_1}{\partial x} + \frac{\partial g_2}{\partial y}\right)(x,y,t^n) + \frac{(\lambda\Delta t^n)^2}{2}\left(\frac{\partial^2 w}{\partial x^2} + \frac{\partial^2 w}{\partial y^2}\right)(x,y,t^n) \\ + \mathcal{O}\left((\Delta t^n)^3\right). \end{aligned} \tag{4.4}$$

Remark 4.1. Notice that in the limit $\Delta t^n \to 0$, the above equation (4.4) yields the modified partial differential equation for the scheme (3.5). It is easy to see that in the resulting equation the diffusion term is of $\mathcal{O}(\Delta t^n)$, as in the classical kinetic schemes.

We can now rewrite the second order Taylor expansion (4.2) by adding and subtracting the $\mathcal{O}\left((\Delta t^n)^2\right)$ term appearing in (4.4) to get

$$\begin{aligned} w(x,y,t^n+\Delta t^n) = w(x,y,t^n) - \Delta t^n\left(\frac{\partial g_1}{\partial x} + \frac{\partial g_2}{\partial y}\right)(x,y,t^n) + \frac{(\lambda\Delta t^n)^2}{2}\left(\frac{\partial^2 w}{\partial x^2} + \frac{\partial^2 w}{\partial y^2}\right)(x,y,t^n) \\ - \frac{(\Delta t^n)^2}{2}\left[\frac{\partial}{\partial x}\left\{\left(\lambda^2 I - A_1^2\right)\frac{\partial w}{\partial x} - A_1A_2\frac{\partial w}{\partial y}\right\} + \frac{\partial}{\partial y}\left\{-A_2A_1\frac{\partial w}{\partial x} + \left(\lambda^2 I - A_2^2\right)\frac{\partial w}{\partial y}\right\}\right] \\ (x,y,t^n) + \mathcal{O}\left((\Delta t^n)^3\right). \end{aligned} \tag{4.5}$$

Note that the first three terms in the above equation (4.5) are coming from the first order scheme (3.5). We can give a physical meaning to the last term involving $(\Delta t^n)^2$. For this, let us first define the matrices

$$\mathcal{B}_{11} := \lambda^2 I - A_1^2,\ \mathcal{B}_{12} := -A_1A_2,\ \mathcal{B}_{21} := -A_2A_1,\ \mathcal{B}_{22} := \lambda^2 I - A_2^2, \tag{4.6}$$

where I denotes the 4×4 identity matrix. The matrices $\mathcal{B}_{ij}$ have the generic form, cf. (2.16)

$$\mathcal{B}_{ij}(w) = \sum_{k=1}^{4} a_i(k)a_j(k)M_k'(w) - A_i(w)A_j(w), \quad i,j = 1,2. \tag{4.7}$$

With the aid of these matrices $\mathcal{B}_{ij}$, we can define

$$\mathcal{D}_1 := -\frac{\Delta t^n}{2}\left(\mathcal{B}_{11}\frac{\partial w}{\partial x} + \mathcal{B}_{12}\frac{\partial w}{\partial y}\right), \ \mathcal{D}_2 := -\frac{\Delta t^n}{2}\left(\mathcal{B}_{21}\frac{\partial w}{\partial x} + \mathcal{B}_{22}\frac{\partial w}{\partial y}\right). \tag{4.8}$$

Thus, (4.5) can be recast in the equivalent, but compact, form

$$w(x,y,t^n+\Delta t^n) = \sum_{k=1}^{4} M_k\left(w^n(x-a_1(k)\Delta t^n, y-a_2(k)\Delta t^n)\right) + \Delta t^n\left(\frac{\partial \mathcal{D}_1}{\partial x} + \frac{\partial \mathcal{D}_2}{\partial y}\right) + \mathcal{O}\left((\Delta t^n)^3\right), \tag{4.9}$$

which is the required second order extension of the kinetic relaxation scheme (3.5).

The results in [1, 5] guarantees that under the stability condition (2.13), the matrices $\mathcal{B}_{ij}$ in (4.7) are all nonnegative definite. Hence, both $\mathcal{D}_1$ and $\mathcal{D}_2$ behave like viscous stress terms with B_{ij} as the corresponding diffusion matrices. These new stress terms $\mathcal{D}_1$ and $\mathcal{D}_2$ are the analogues of the heat flux vector and viscous stress obtained by Deshpande [8], for the compressible Euler equations, in the context of classical kinetic schemes. The gradients $\partial\mathcal{D}_1/\partial x$ and $\partial\mathcal{D}_2/\partial y$ will therefore act as dissipative fluxes. The crucial point to note here is that the signs of $\mathcal{D}_1$ and $\mathcal{D}_2$ in (4.8) are negative. As a result, both the terms $\partial\mathcal{D}_1/\partial x$ and $\partial\mathcal{D}_2/\partial y$ in (4.9) are negative diffusive fluxes, or in other words, they are anti-diffusive fluxes. We have already pointed out that the first term in (4.9) is coming from the first order scheme (3.5). Hence, in order to achieve second order time accuracy for the discrete kinetic scheme (3.13), we need to consider not only the upwind relaxation term but also the anti-diffusive terms. In addition to serving as second order corrections, the anti-diffusive terms also reduces the excess amount of numerical diffusion present in the first order upwind relaxation scheme (3.13).

It is well known that the Maxwellian equilibrium distributions of the type $M_k(w)$ gives an inviscid system of conservation laws in the hydrodynamic limit, e.g. see [5, 7]. However, in the second order scheme (4.9) we have incorporated diffusive flux terms. Therefore, in order to get dissipative flux like terms $\partial\mathcal{D}_1/\partial x$ and $\partial\mathcal{D}_2/\partial y$ we need to change the Maxwellian distribution to the so-called Chapman-Enskog distribution. The latter is always associated with diffusion equations, such as the Navier-Stokes equations and hence it can give rise to nonzero viscous terms. Moreover, the method of replacing the time derivatives by space derivatives we performed to derive (4.2) is also a characteristic of the Chapman-Enskog procedure. In what follows, we derive a Chapman-Enskog distribution and examine its relation to the second order accurate scheme (4.9).

From the BGK Boltzmann equation (2.11) we infer that $M_k(w_f) - f_k = \mathcal{O}(\epsilon)$ and as a result

$$\begin{aligned} f_k &= M_k(w_f) - \epsilon\left\{\frac{\partial f_k}{\partial t} + a_1(k)\frac{\partial f_k}{\partial x} + a_2(k)\frac{\partial f_k}{\partial y}\right\}, \\ &= M_k(w_f) - \epsilon\left\{\frac{\partial M_k(w_f)}{\partial t} + a_1(k)\frac{\partial M_k(w_f)}{\partial x} + a_2(k)\frac{\partial M_k(w_f)}{\partial y}\right\} + \mathcal{O}\left(\epsilon^2\right). \end{aligned} \tag{4.10}$$

Note that the right hand side of (4.10) is a perturbation of the Maxwellian M_k. Motivated by this, the Chapman-Enskog distribution function $\tilde{M}_k$ is defined by

$$\tilde{M}_k(w) := M_k(w) - \tau\left\{\frac{\partial M_k(w)}{\partial t} + a_1(k)\frac{\partial M_k(w)}{\partial x} + a_2(k)\frac{\partial M_k(w)}{\partial y}\right\}, \tag{4.11}$$

where τ is a parameter to be determined. Analogous to the consistency conditions (2.12), the Chapman-Enskog distribution function $\tilde{M}_k(w)$ is required to satisfy the moment relations

$$\sum_{k=1}^{4} \tilde{M}_k(w) = w, \ \sum_{k=1}^{4} a_1(k)\tilde{M}_k(w) = g_1(w) + \mathcal{D}_1, \ \sum_{k=1}^{4} a_2(k)\tilde{M}_k(w) = g_2(w) + \mathcal{D}_2. \tag{4.12}$$

Note that the first relation in (4.12) is the conservation property. The second and third relations precisely state that unlike the Maxwellian, the Chapman-Enskog distribution should give a nonzero viscous flux in addition to the inviscid flux. We can now obtain the precise form $\tilde{M}_k(w)$ by evaluating the expressions in curly brackets on the right hand side of (4.11), e.g. we get from (2.16)

$$\frac{\partial M_1}{\partial t} = \frac{1}{4}\frac{\partial w}{\partial t} - \frac{1}{4\lambda}\frac{\partial g_1(w)}{\partial t} - \frac{1}{4\lambda}\frac{\partial g_2(w)}{\partial t}. \tag{4.13}$$

Using chain rule and the conservation law (2.1) we can replace all the time derivatives by spatial derivatives to get

$$\frac{\partial M_1}{\partial t} = \frac{1}{4\lambda}\left(-\lambda A_1 + A_1^2 + A_1A_2\right)\frac{\partial w}{\partial x} + \frac{1}{4\lambda}\left(-\lambda A_2 + A_1A_2 + A_2^2\right)\frac{\partial w}{\partial y}. \tag{4.14}$$

In an analogous manner we can compute from (2.16)

$$\frac{\partial M_1}{\partial x} = \frac{1}{4\lambda}\left(\lambda I - A_1 - A_2\right)\frac{\partial w}{\partial x}, \ \frac{\partial M_1}{\partial y} = \frac{1}{4\lambda}\left(\lambda I - A_1 - A_2\right)\frac{\partial w}{\partial y}. \tag{4.15}$$

Thus, from (4.13)-(4.15) we finally get

$$\frac{\partial M_1}{\partial t} - \lambda\frac{\partial M_1}{\partial x} - \lambda\frac{\partial M_1}{\partial y} = \frac{1}{4\lambda}\left(A_1^2 + A_2A_1 + \lambda A_2 - \lambda^2 I\right)\frac{\partial w}{\partial x} + \frac{1}{4\lambda}\left(A_1A_2 + A_2^2 + \lambda A_1 - \lambda^2 I\right)\frac{\partial w}{\partial y}. \tag{4.16}$$

Along similar lines we can obtain the relevant factors involving M_2, M_3 and M_4. Assembling all the required expressions in (4.11), it can easily be seen that we must take $\tau = -2/\Delta t^n$ in order to satisfy the second and third relations in (4.12). Thus, from (4.11) we can obtain the Chapman-Enskog distribution function

$$\tilde{M}_1 = M_1 - \frac{\Delta t^n}{8\lambda}\left(A_1^2 + A_2A_1 + \lambda A_2 - \lambda^2 I\right)\frac{\partial w}{\partial x} - \frac{\Delta t^n}{8\lambda}\left(A_1A_2 + A_2^2 + \lambda A_1 - \lambda^2 I\right)\frac{\partial w}{\partial y}, \tag{4.17}$$

$$\tilde{M}_2 = M_2 - \frac{\Delta t^n}{8\lambda}\left(-A_1^2 + A_2A_1 - \lambda A_2 + \lambda^2 I\right)\frac{\partial w}{\partial x} - \frac{\Delta t^n}{8\lambda}\left(-A_1A_2 + A_2^2 - \lambda A_1 - \lambda^2 I\right)\frac{\partial w}{\partial y}, \tag{4.18}$$

$$\tilde{M}_3 = M_3 - \frac{\Delta t^n}{8\lambda}\left(-A_1^2 - A_2A_1 + \lambda A_2 + \lambda^2 I\right)\frac{\partial w}{\partial x} - \frac{\Delta t^n}{8\lambda}\left(-A_1A_2 - A_2^2 + \lambda A_1 + \lambda^2 I\right)\frac{\partial w}{\partial y}, \tag{4.19}$$

$$\tilde{M}_4 = M_4 - \frac{\Delta t^n}{8\lambda}\left(A_1^2 - A_2A_1 - \lambda A_2 - \lambda^2 I\right)\frac{\partial w}{\partial x} - \frac{\Delta t^n}{8\lambda}\left(A_1A_2 - A_2^2 - \lambda A_1 + \lambda^2 I\right)\frac{\partial w}{\partial y}. \tag{4.20}$$

Remark 4.2. It is to be noted that unlike the Maxwellian M_k, the Chapman-Enskog distribution $\tilde{M}_k$ depends also on the derivatives of the conservative variable w. In other words, the support of the Chapman-Enskog distribution is larger than the corresponding Maxwellian.

We can give an interpretation of the second order scheme as coming from an initial value problem of the type (3.2)-(3.3), with the exception that the initial value of f_k is $\tilde{M}_k$ instead of M_k, i.e.

$$f_k(x, y, t^n) = \tilde{M}_k(w^n(x, y)). \tag{4.21}$$

The solution of the transport equation (3.2) with the above initial datum is clearly

$$f_k(x, y, t^n + \Delta t^n) = \tilde{M}_k\left(w^n(x - a_1(k)\Delta t^n, y - a_2(k)\Delta t^n)\right). \tag{4.22}$$

Taking moments we get

$$w(x,y,t^n+\Delta t^n) = \sum_{k=1}^{4} \tilde{M}_k \left(w^n(x-a_1(k)\Delta t^n, y-a_2(k)\Delta t^n) \right). \tag{4.23}$$

Expanding the right hand side of the above equation (4.23) in the Taylor series and using the moment relations (4.12), it can be seen that we recover the second order scheme (3.5). Thus, (4.23) is the upwind version of (3.5) with the Chapman-Enskog distribution instead of the Maxwellian.

4.2. **Second Order Accuracy in Space.** Our next aim is to achieve second order accuracy in space. The equation (4.9) shows that in the second order scheme also the values of M_k are to be evaluated at non-mesh points. Since the anti-diffusive correction terms are $\mathcal{O}((\Delta t^n)^2)$, we need to evaluate the first term in (4.9) to second order accuracy. Therefore, like the first order scheme we should employ an interpolation procedure, but which should be second order accurate. Note that in our first order scheme, we have used a bilinear interpolation method for this purpose and the overall scheme turned out to be positivity preserving. This is due to the fact that the bilinear interpolation formulae in (3.9)-(3.12) can be written as convex linear combinations of the values of the Maxwellian densities $M_k(w)$. Thus, when using a second order interpolation instead of (3.9)-(3.12), we must ensure that the interpolated values should not give any non-physical negative density or pressure.

A second order interpolation method can be easily obtained by replacing the first order interpolation formulae (3.9)-(3.12) by corresponding second order difference formulae, e.g.

$$\begin{aligned} {f_1}_{i,j}^{n+1} = {M_1}_{i,j}^{n} &+ \frac{\eta_1}{2}\left(\delta_x^+ + \delta_x^-\right){M_1}_{i,j}^{n} + \frac{\eta_1^2}{2}\left(\delta_x^+ - \delta_x^-\right){M_1}_{i,j}^{n} \\ &+ \frac{\eta_2}{2}\left(\delta_y^+ + \delta_y^-\right){M_1}_{i,j}^{n} + \frac{\eta_2^2}{2}\left(\delta_y^+ - \delta_y^-\right){M_1}_{i,j}^{n} + \eta_1\eta_2\delta_x^+\delta_y^+{M_1}_{i,j}^{n}. \end{aligned} \tag{4.24}$$

However, it is not possible to write the expression on the right hand side as a convex combination of the values of M_1 in the stencil. In addition, the density and energy components of the above vector valued interpolated expression need not be positive even if the corresponding values of M_1 at the mesh points are positive. This is particularly true in the presence of shocks and other high gradients, where the second order slopes can have wild variation. This gives an indication that in (4.24) we must use some limiter type functions to suppress the oscillations and unphysical values. We recast (4.24) in an alternate form

$$\begin{aligned} {f_1}_{i,j}^{n+1} = {M_1}_{i,j}^{n} &+ \eta_1\delta_x^+{M_1}_{i,j}^{n} + \eta_2\delta_y^+{M_1}_{i,j}^{n} + \eta_1\eta_2\delta_x^+\delta_y^+{M_1}_{i,j}^{n} \\ &- \frac{\eta_1}{2}(1-\eta_1)\left(\delta_x^+ - \delta_x^-\right){M_1}_{i,j}^{n} - \frac{\eta_2}{2}(1-\eta_2)\left(\delta_y^+ - \delta_y^-\right){M_1}_{i,j}^{n}. \end{aligned} \tag{4.25}$$

Note that the first four terms together gives the first order bilinear interpolation formula. Since the first order formula is positivity preserving and non-oscillatory, we must switch over to it in the presence of high gradients. However, we must use the second order interpolation scheme in smooth regions of the flow in order to achieve second order accuracy in space. This can be achieved with the use of an adaptive parameter, say χ, so that in equilibrium or smooth flow regions $\chi \sim 0$ and in discontinuity region $\chi \sim 1$. We limit the second order contribution terms in (4.25) to get

$$\begin{aligned} {f_1}_{i,j}^{n+1} = {M_1}_{i,j}^{n} &+ \eta_1\delta_x^+{M_1}_{i,j}^{n} + \eta_2\delta_y^+{M_1}_{i,j}^{n} + \eta_1\eta_2\delta_x^+\delta_y^+{M_1}_{i,j}^{n} \\ &- \frac{\eta_1}{2}(1-\eta_1)\chi_1\left(\delta_x^+ - \delta_x^-\right){M_1}_{i,j}^{n} - \frac{\eta_2}{2}(1-\eta_2)\chi_2\left(\delta_y^+ - \delta_y^-\right){M_1}_{i,j}^{n}. \end{aligned} \tag{4.26}$$

Here, χ_1 and χ_2 are appropriate discontinuity indicators and we have used the switching function of the JST scheme [12] for this purpose, i.e.

$$\chi_1 = \frac{|p^n_{i+1,j} - 2p^n_{i,j} + p^n_{i-1,j}|}{|p^n_{i+1,j} + 2p^n_{i,j} + p^n_{i-1,j}|}, \tag{4.27}$$

with an analogous definition for χ_2. Along similar lines, we can define the second order interpolated values of M_2, M_3 and M_4.

Remark 4.3. It has to be noted that in the second order kinetic schemes of [8, 15] different interpolation and limiting strategies were employed . However, our numerical experiments confirm the non-oscillatory nature of the interpolation method of the type (4.26).

To complete the second order scheme we need to evaluate also the anti-diffusive flux terms $\partial\mathcal{D}_1/\partial x$ and $\partial\mathcal{D}_1/\partial y$. Note that the evaluation of $\mathcal{D}_1$ and $\mathcal{D}_2$ requires the computation of the slopes $\partial w/\partial x$ and $\partial w/\partial y$. As explained above, when strong discontinuities, such as shocks and contacts are present in the solution, these gradients can have very drastic variation. This can also lead the second order scheme (4.9) to give some unphysical solutions. Therefore, we must apply some nonlinear limiter functions also in the calculation of the these gradients. A possible computation of such slopes, which results in an overall non-oscillatory scheme is given by a family of discrete derivatives parametrised by $1 \leq \theta \leq 2$, e.g.

$$\frac{\partial w}{\partial x}(x_i, y_j, t^n) = MM\left(\theta\frac{w^n_{i+1,j} - w^n_{i,j}}{\Delta x}, \frac{w^n_{i+1,j} - w^n_{i-1,j}}{2\Delta x}, \theta\frac{w^n_{i,j} - w^n_{i-1,j}}{\Delta x}\right) \tag{4.28}$$

with an analogous expression for the y-slope. Here, MM denotes the nonlinear minmod function defined by

$$MM\left\{x_1, x_2, \cdots\right\} = \begin{cases} \min_p\{x_p\} & \text{if } x_p > 0 \ \forall p, \\ \max_p\{x_p\} & \text{if } x_p < 0 \ \forall p, \\ 0 & \text{otherwise.} \end{cases} \tag{4.29}$$

After computing the values of $\mathcal{D}_1$ and $\mathcal{D}_2$ at all the mesh points, the derivatives $\partial\mathcal{D}_1/\partial x$ and $\partial\mathcal{D}_1/\partial y$ are also calculated using the same minmod recovery procedure. Thus, we have completed the evaluation of all the terms required by the second order scheme (4.9).

5. Numerical Results

In this section we present the results of our numerical experiments on some benchmark problems for the Euler equations. We consider a range of test-problems and demonstrate the second order convergence of the scheme and its ability to capture genuine multidimensional flow features.

5.1. **Experimental order of convergence.** In order to numerically verify the second order convergence of the scheme (4.9) we compute the experimental order of convergence (EOC) for a smooth solution. We consider a smooth periodic solution of the 2-D Euler equations, given by

$$\begin{aligned} \rho(x, y, t) &= 1.0 + 0.5 \sin\left(\pi(x + y - t(u + v))\right), \\ u(x, y, t) &= v(x, y, t) = p(x, y, t) = 1.0. \end{aligned}$$

The EOC can be calculated by systematically refining the mesh and examining the behaviour of the global error. Since the exact solution is known, the order of convergence in a certain norm $\|\cdot\|$ can be computed in the following way

$$\text{EOC} = \log_2\left(\frac{\|w^n_{N/2} - w^n_{ref}\|}{\|w^n_N - w^n_{ref}\|}\right),$$

where N denotes the number of mesh points in both x- and y- directions, w denotes the approximate and w_{ref} the exact solution. A suitable choice for the norm $\|\cdot\|$ is L^1, L^2 or L^∞. The computational domain $[-1,1]\times[-1,1]$ is consecutively divided into 20×20, $40\times 40,\ldots,320\times 320$ cells. The final time was taken to be $t=0.1$. In order to evaluate the upwind relaxation term in (4.9) we use the second order interpolation formulae, such as (4.24) and the Chapman-Enskog terms $\mathcal{D}_1, \mathcal{D}_2$ and their derivatives are computed using central differences without any limiters. The table 1 shows the experimental order of convergence calculated in the three norms. It is evident from the table that the order of convergence is two.

N	L^1 error	EOC	L^2 error	EOC	L^∞ error	EOC
20	0.01801515		0.01993357		0.02794240	
40	0.00332742	2.43673590	0.00369252	2.43252224	0.00521205	2.42253293
80	0.00071280	2.22284153	0.00079185	2.22130172	0.00111969	2.21875624
160	0.00016955	2.07173835	0.00018834	2.07189826	0.00026609	2.07310876
320	0.00004183	2.01916530	0.00004647	2.01882292	0.00006616	2.00786708

TABLE 1. L^1, L^2 and L^∞ errors with EOC for a smooth periodic test case.

5.2. **Cylindrical Explosion Problem.** The first test case is a two-dimensional Sod problem with a circular discontinuity. The computational domain is the square $[-1,1]\times[-1,1]$ and the initial data read,

$$(\rho,u,v,p)(x,y,0)=\begin{cases}(1,0,0,1) & \text{if } \sqrt{x^2+y^2}<0.4,\\ (0.125,0,0,0.1) & \text{otherwise.}\end{cases}$$

The solution is computed at time $t=0.2$ on a 400×400 mesh with a CFL number 0.45 using the second order accurate method. The solution exhibits a circular shock and a circular contact discontinuity moving away from the centre of the circle and a circular rarefaction wave moving in the opposite direction. In this problem we have used absorbing boundary conditions by simple zeroth order extrapolation of the variables. The isolines of density, x-, y- components of velocity and pressure are given in figure 2. It is evident from figure 2 that the scheme resolves circular shocks and contacts very accurately, confirming its genuinely multidimensional nature.

5.3. **2-D Riemann Problems.** Next test case is a two-dimensional Riemann problem. The computational domain $[-1,1]\times[-1,1]$ is divided into four quadrants. The initial data consist of single constant states in each of these four quadrants. These constant values are chosen in such a way that each pair of quadrants defines a one-dimensional Riemann problem.

We choose the initial values in such a way that two forward moving shocks and two standing slip lines are produced. The initial data read,

$$(\rho,u,v,p)(x,y,0)=\begin{cases}(0.5313,0.0,0.0,0.4) & \text{if } x>0,\ y>0,\\ (1.0,0.0,0.7276,1.0) & \text{if } x>0,\ y<0,\\ (1.0,0.7276,0.0,1.0) & \text{if } x<0,\ y>0,\\ (0.8,0.0,0.0,1.0) & \text{if } x<0,\ y<0.\end{cases}$$

The solution is computed at time $t=0.52$ with a CFL number 0.45 with both first order and second order methods. The isolines of the density is given in figure 3. It is evident from the figure that the second order method is far less dissipative than the first order scheme. Moreover, the second order scheme resolves the shocks and slip lines very accurately.

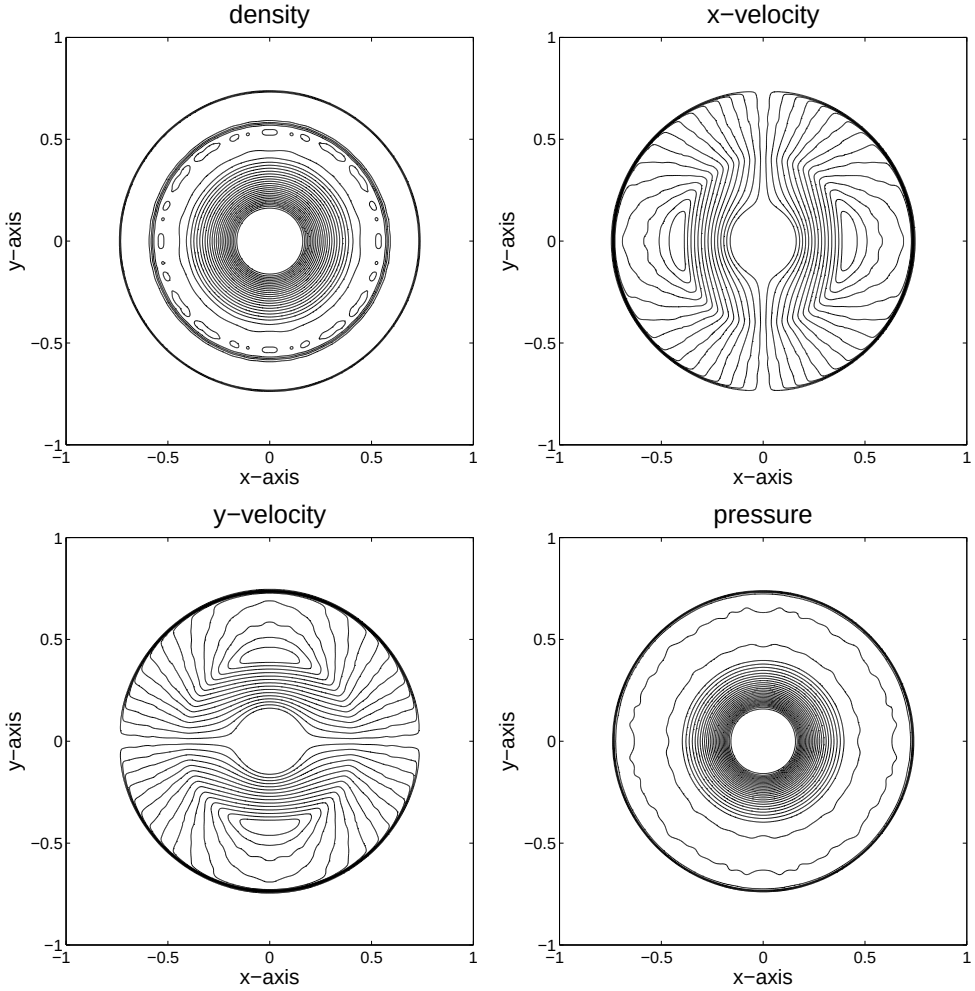

FIGURE 2. Cylindrical explosion problem. Isolines of the solution obtained by the second order scheme at $t = 0.2$ on a 400×400 mesh.

5.4. **Double Mach Reflection Problem.** This test case is the double Mach reflection problem studied in [30]. The computational domain is $[0, 4] \times [0, 1]$ and the setup is as follows. A reflecting wall lies at the bottom of the domain starting at $x = \frac{1}{6}$. Initially, a right moving shock is situated at the point $(\frac{1}{6}, 0)$, with the shock making an angle 60° with the x-axis. At the bottom boundary, the postshock values are values are imposed for the region from $x = 0$ to $x = \frac{1}{6}$ and reflecting boundary conditions for the rest. On the top boundary, all the flow parameters specified to represent the exact motion of a Mach 10 shock. The left boundary is an inflow boundary, whereas the right boundary is outflow. The isolines of the density and pressure computed on a 240×60 mesh with the second order scheme is given in figure 4. It is clear that the our scheme resolve the complex flow features of this problem quite well.

5.5. **Shock Bubble Interaction Problem.** The simulations in this example shows the interaction between a planar shock and various heterogeneity. The motivation for this problem is the 3-D shock bubble interaction studied by Langseth and LeVeque [16]. The problem setup is as follows. A bubble of radius 0.2 lies at rest at $(0.4, 0.5)$ in the domain $[0, 1.6] \times [0, 1]$. The gas is at rest initially and has

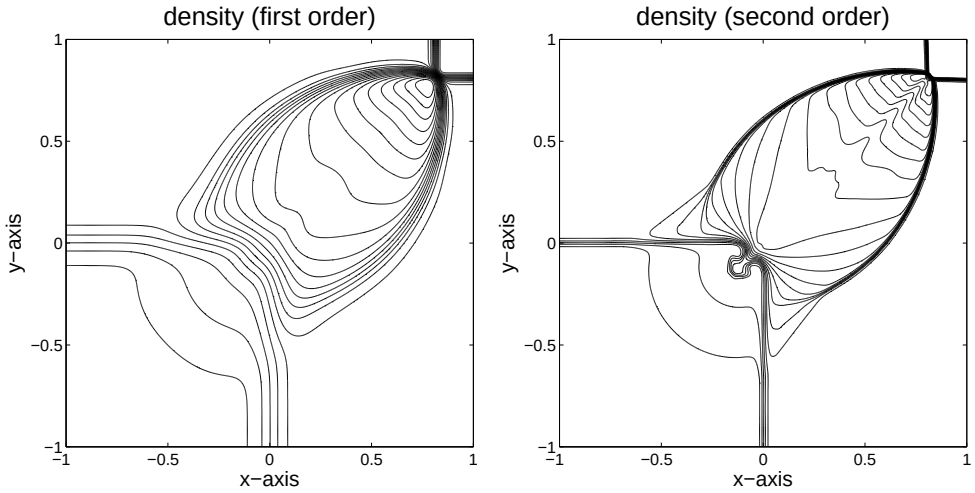

FIGURE 3. 2-D Riemann problem with two shocks and two slip lines. Isolines of the density computed using the first order and second order schemes at time $t = 0.52$ on a 400×400 mesh.

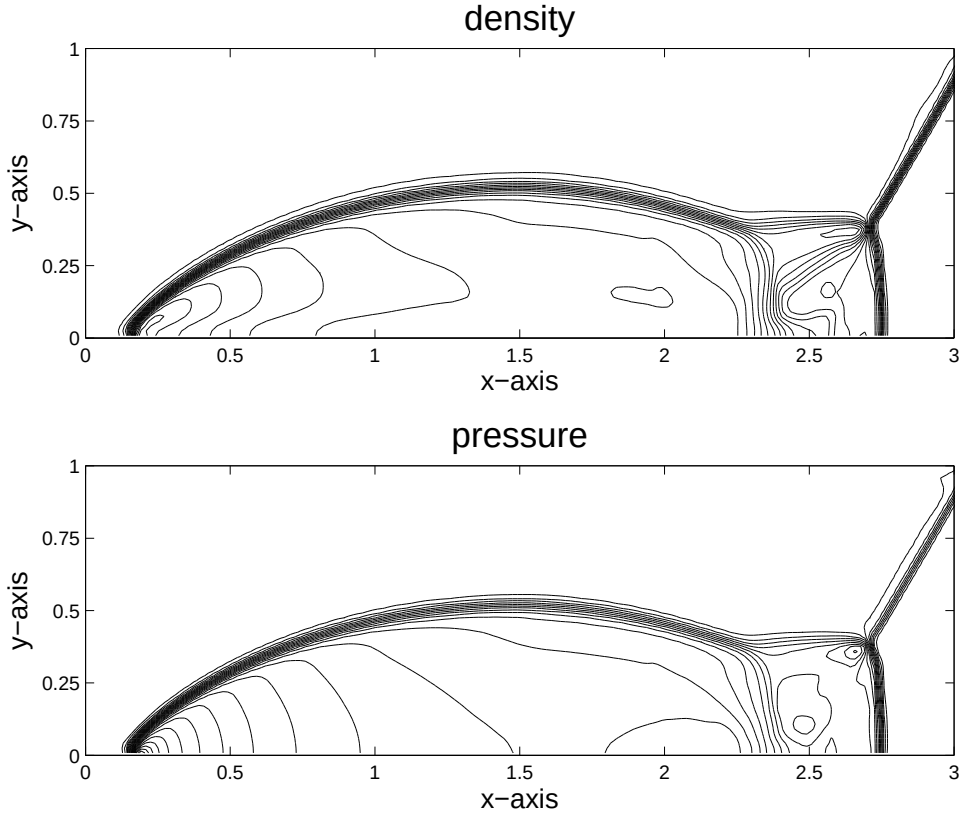

FIGURE 4. Double Mach reflection problem. Density and pressure isolines at time $t = 0.2$ computed on a 240×60 mesh.

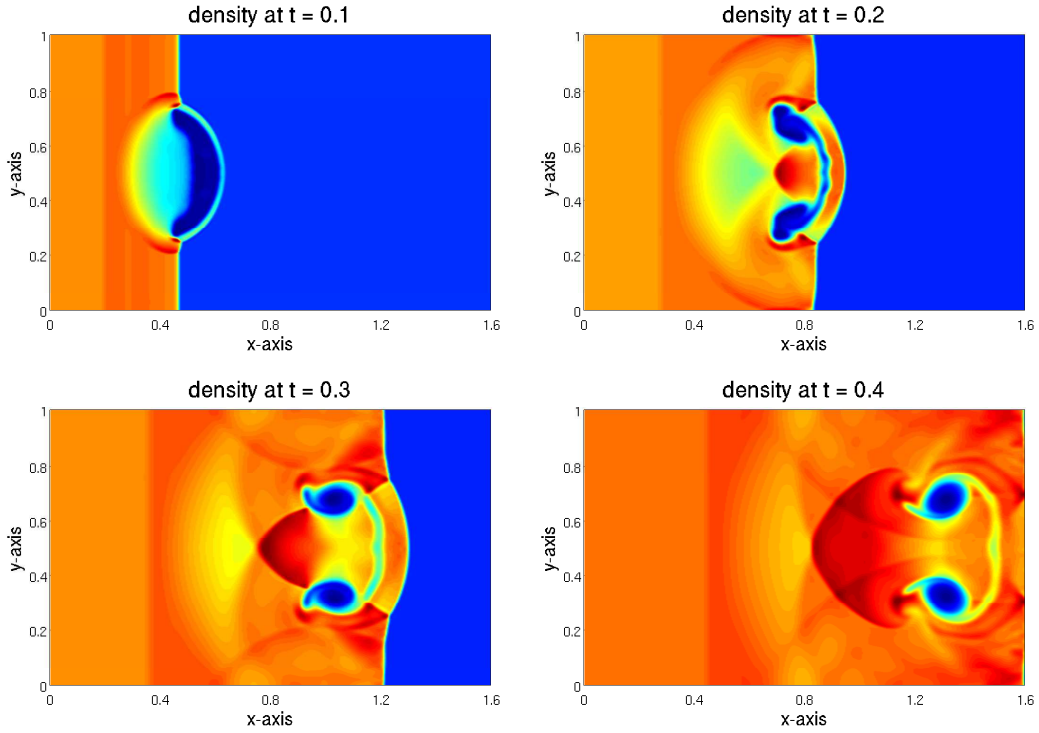

FIGURE 5. Shock-bubble interaction problem: pseudo-colour images of the density at different times from $t = 0.1$ to $t = 0.4$ calculated with second order scheme on a 640×400 mesh.

unit density and pressure. The density inside the bubble is 0.1 while the velocities and pressure has same values as outside. The incoming shock wave starts at $x = 0.1$ and propagates in the positive x-direction. Behind the shock the density is 3.81, pressure is 10, x-velocity is 2.85 and y-velocity is 0. The pseudo-colour images of the density for different time from $t = 0.1$ to $t = 0.4$ is given in figure 5. We have used reflecting boundary conditions on the top and bottom boundaries. The right boundary has outflow boundary conditions whereas the left is inflow boundary.

6. Concluding Remarks

A novel genuinely multidimensional discrete kinetic scheme based on a relaxation system in which the foot of the characteristics traverses all quadrants in an isotropic way is proposed for the solution of a hyperbolic system of conservation in two dimensions. The scheme achieves second order time by the use of an anti-diffusive Chapman-Enskog distribution function instead of the Maxwellian, whereas the second order space accuracy is achieved using second order interpolation with limiters to avoid oscillations. The proposed scheme is validated against a set of well-known benchmark problems for the Euler equations in two dimensions and the results demonstrate second order convergence and its efficiency to capture the flow features accurately. The extension of the present scheme to other complex hyperbolic systems is straightforward. The discrete kinetic relaxation scheme also retains many attractive features of the central schemes, such as neither Riemann solvers nor characteristic decompositions are needed.

Acknowledgements

The authors thank Professors Sebastian Noelle and Phoolan Prasad for their constant encouragement and support. K. R. A. gratefully acknowledges the Alexander von Humboldt Foundation for a postdoctoral fellowship.

References

[1] D. Aregba-Driollet and R. Natalini. Discrete kinetic schemes for multidimensional systems of conservation laws. *SIAM J. Numer. Anal.*, 37:1973–2004, 2000.

[2] K. R. Arun, M. Kraft, M. Lukáčová-Medviďová, and P. Prasad. Finite volume evolution Galerkin method for hyperbolic conservation laws with spatially varying flux functions. *J. Comput. Phys.*, 228:565–590, 2009.

[3] K. R. Arun, M. Lukáčová-Medviďová, P. Prasad, and S. V. Raghurama Rao. A second order accurate kinetic relaxation scheme for inviscid compressible flows. Technical report, Department of Mathematics, Indian Institute of Science, Bangalore, 2010. Available on http://math.iisc.ernet.in/prasad/.

[4] P. L. Bhatnagar, E. P. Gross, and M. Krook. A model for collision processes in gases. I. Small amplitude processes in charged and neutral one-component systems. *Phys. Rev.*, 94:511–525, 1954.

[5] F. Bouchut. Construction of BGK models with a family of kinetic entropies for a given system of conservation laws. *J. Statist. Phys.*, 95:113–170, 1999.

[6] C. Cercignani. *The Boltzmann equation and its applications*, volume 67 of *Applied Mathematical Sciences*. Springer Verlag, New York, 1988.

[7] G. Q. Chen, C. D. Levermore, and T.-P. Liu. Hyperbolic conservation laws with stiff relaxation terms and entropy. *Comm. Pure Appl. Math.*, 47:787–830, 1994.

[8] S. M. Deshpande. A second order accurate, kinetic-theory based, method for inviscid compressible flows. Technical Report 2613, NASA, Langley, 1986.

[9] S. M. Deshpande. Kinetic flux splitting schemes. In M. Hafez and K. Oshima, editors, *Computational Fluid Dynamics Review 1995: a State-of-the-art Reference to the Latest Developments in CFD*. Wiley, 1995.

[10] M. Fey. Multidimensional upwinding. II. Decomposition of the Euler equations into advection equations. *J. Comput. Phys.*, 143:181–199, 1998.

[11] E. Godlewski and P.-A. Raviart. *Numerical approximation of hyperbolic systems of conservation laws*, volume 118 of *Applied Mathematical Sciences*. Springer-Verlag, New York, 1996.

[12] A. Jameson, W. Schmidt, and E. Turkel. Numerical solution of the euler equations by finite volume methods using Runge Kutta time stepping schemes. *AIAA Paper 81-1259*, 1981.

[13] S. Jin. Runge-Kutta methods for hyperbolic conservation laws with stiff relaxation terms. *J. Comput. Phys.*, 122:51–67, 1995.

[14] S. Jin and Z. P. Xin. The relaxation schemes for systems of conservation laws in arbitrary space dimensions. *Comm. Pure Appl. Math.*, 48:235–276, 1995.

[15] M. Kunik, S. Qamar, and G. Warnecke. Second-order accurate kinetic schemes for the ultra-relativistic Euler equations. *J. Comput. Phys.*, 192:695–726, 2003.

[16] J. O. Langseth and R. J. LeVeque. A wave propagation method for three-dimensional hyperbolic conservation laws. *J. Comput. Phys.*, 165:126–166, 2000.

[17] R. J. LeVeque. *Finite Volume Methods for Hyperbolic Problems*. Cambridge Texts in Applied Mathematics. Cambridge University Press, Cambridge, 2002.

[18] R. J. LeVeque and R. Walder. Grid alignment effects and rotated methods for computing complex flows in astrophysics. In *Proceedings of the Ninth GAMM-Conference on Numerical Methods in Fluid Mechanics (Lausanne, 1991)*, volume 35 of *Notes Numer. Fluid Mech.*, pages 376–385, Braunschweig, 1992. Vieweg.

[19] T.-P. Liu. Hyperbolic conservation laws with relaxation. *Comm. Math. Phys.*, 108:153–175, 1987.

[20] M. Lukáčová-Medviďová, K. W. Morton, and G. Warnecke. Finite volume evolution Galerkin (FVEG) methods for hyperbolic problems. *SIAM J. Sci. Comput.*, 26:1–30, 2004.

[21] R. Natalini. Recent results on hyperbolic relaxation problems. In *Analysis of systems of conservation laws (Aachen, 1997)*, volume 99 of *Chapman & Hall/CRC Monogr. Surv. Pure Appl. Math.*, pages 128–198. Chapman & Hall/CRC, Boca Raton, FL, 1999.

[22] S. Noelle. The MoT-ICE: a new high-resolution wave-propagation algorithm for multidimensional systems of conservation laws based on Fey's method of transport. *J. Comput. Phys.*, 164:283–334, 2000.

[23] S. W. C. Noelle. On the limits of operator splitting: numerical experiments for the complex Burgers equation. Technical Report TR-91-03, Konrad-Zuse-Zentrum für Informationstechnik, Berlin, 1991.

[24] L. Pareschi and G. Russo. Implicit-Explicit Runge-Kutta schemes and applications to hyperbolic systems with relaxation. *J. Sci. Comput.*, 25:129–155, 2005.
[25] B. Perthame. Boltzmann type schemes for gas dynamics and the entropy property. *SIAM J. Numer. Anal.*, 27:1405–1421, 1990.
[26] B. Perthame. Second-order Boltzmann schemes for compressible Euler equations in one and two space dimensions. *SIAM J. Numer. Anal.*, 29:1–19, 1992.
[27] P. L. Roe. Discrete models for the numerical analysis of time-dependent multidimensional gas dynamics. *J. Comput. Phys.*, 63:458–476, 1986.
[28] G. R. Shubin and J. B. Bell. An analysis of the grid orientation effect in numerical simulation of miscible displacement. *Comput. Meth. Appl. Mech. Eng.*, 47:47–71, 1984.
[29] E. Tadmor. Approximate solutions of nonlinear conservation laws. In *Advanced numerical approximation of nonlinear hyperbolic equations (Cetraro, 1997)*, volume 1697 of *Lecture Notes in Math.*, pages 1–149. Springer, Berlin, 1998.
[30] P. Woodward and P. Colella. The numerical simulation of two-dimensional fluid flow with strong shocks. *J. Comput. Phys.*, 54:115–173, 1984.
[31] K. Xu. Gas kinetic scheme for unsteady compressible flow simulations. In *Lecture Note Series 1998-03*. Von Kárman Institute for Fluid Dynamics, Rhode Saint Genèse, Belgium, 1998.

Institut für Geometrie und Praktische Mathematik, RWTH-Aachen, Templergraben 55, D-52056 Aachen, Germany.
E-mail address: arun@igpm.rwth-aachen.de

Institut für Mathematik, Johannes Gutenberg-Universität Mainz, Staudingerweg 9, D-55099 Mainz, Germany.
E-mail address: lukacova@mathematik.uni-mainz.de
URL: http://www.mathematik.uni-mainz.de/Members/lukacova